Journal of Molecular Structure 1179 (2019) 65–75

Contents lists available at ScienceDirect

Journal of Molecular Structure

journal homepage: http://www.elsevier.com/locate/molstruc

Synthesis, structural investigations, DFT, molecular docking and antifungal studies of transition metal complexes with benzothiazole based Schiff base ligands

Ranjan K. Mohapatra [a], Ashish K. Sarangi [a, *], Mohammad Azam [b], Marei M. El-ajaily [c], Md Kudrat-E-Zahan [d], Suyanbhu B. Patjoshi [e], Dhruba C. Dash [e]

[a] Department of Chemistry, Government College of Engineering, Keonjhar, 758002, Odisha, India
[b] Department of Chemistry, College of Science, King Saud University, Riyadh, Saudi Arabia
[c] Chemistry Department, Faculty of Science, Benghazi University, Benghazi, Libya
[d] Department of Chemistry, Rajshahi University, Rajshahi, 6205, Bangladesh
[e] School of Chemistry, Sambalpur University, Jyoti Vihar, Sambalpur, 768019, Odisha, India

ARTICLE INFO

Article history:
Received 15 August 2018
Received in revised form
28 September 2018
Accepted 22 October 2018
Available online 24 October 2018

Keywords:
Schiff base
Complexes
DFT
Molecular docking
Antifungal studies

ABSTRACT

A novel series of complexes of the type, $[ML_2].nH_2O$, [where L = 2-(α-methyl salicylidene−2′-imino) aminobenzo thiazole (HMAB), 2-(α-phenyl salicylidene−2′-imino) aminobenzo thiazole (HPAB), 2-(o-Vanillidene−2′-imino) amino benzothiazole (HVAB)] have been reported. These Schiff bases and their transition metal complexes were fully characterized by several physico-chemical and spectral techniques, which revealed the tridentate chelation of ligand. The DFT calculations of these reported compounds were made to obtain bonding inside the structure by GAUSSIAN 03 programme platforms. The QSAR study was performed by HyperChem Professional 8.0.3 software to explain the biological effeteness of the ligands. A docking analysis using the AutoDock Vina software was carried out to understand the binding pattern of the investigated compounds towards target proteins CYP121 and CYP51 from *Mycobacterium tuberculosis*. Furthermore, all the compounds have been reported to exhibit significant antifungal activity when tested against *Aspergillus flavus and Aspergillus niger.*

1. Introduction

Coordination chemistry provides us large number of interesting and useful complexes by the use of organic ligands containing hetero atoms as coordination sites. Furthermore, the ligands with more than one donor hetero atoms have received worldwide attention in coordination chemistry because of their strong chelating ability to form mono-, di- or multinuclear complexes [1,2]. In addition, the lone pair of electrons available on hetero atoms participates strongly in the formation of metal-ligand bonds.

Over the years, heterocyclic ligands with 'NOS' donor atoms especially benzothiazoles have received significant attention due to their unique complex forming ability and huge applications in analytical chemistry as spectrometric and gravimetric reagents.

Benzothiazole, a sulphur isostere of benzimidazole, is a well-known heterocyclic moiety with remarkable physical and biological properties. Furthermore, benzothiazoles and its derivatives find extensive role in medicinal chemistry such as antimicrobial [3,4], antitumor [5], anthelmintic [6], anticancer [7], antifungal [8,9], anti-HIV [10] and antitubercular agent [11]. In addition, benzothiazole and its derivatives are also reported showing luminescence properties [12] and have been used as anti-diabetes agent and central muscle relaxants [13]. Furthermore, it is reported that the activity of such compounds is increased when administered as metal complexes.

In continuation of our ongoing interest on coordination chemistry [14,15], we are reporting some benzothiazole derived Schiff bases with −OH, $-OCH_3$ functional groups vicinal to condensation site and their complexes with metals ions of first transition series.

* Corresponding author.
E-mail address: ashishsbp_2008@yahoo.com (A.K. Sarangi).

https://doi.org/10.1016/j.molstruc.2018.10.070
0022-2860/

In addition, to obtain insight into the structure of the ligands and their metal complexes, DFT calculations have been carried out. Furthermore, the bio-potency of these compounds has been examined against *A. flavus and A. niger.*

2. Experimental

2.1. Material

All chemicals and reagents including 2-mercepto benzothiazole, hydrazine hydrate, o-hydroxy acetophenone, o-hydroxy benzophenone, o-vanillin and the metal salts were of Sigma Aldrich and used without further purification.

2.2. Procedure for the synthesis of 2-hydrazinobenzothiazole

2 mL hydrazine hydrate was added to a hot ethanolic (30 mL) solution of 2-mercepto benzothiazole (1.67 gm, 50 mmol). The reaction mixture was refluxed for around 4 h until H_2S gas ceased to evolve. It was cooled at room temperature, and left for evaporation. After few days, white needle shaped crysatalline material is obtained.

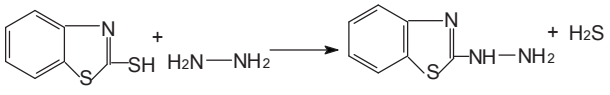

(2-mercepto benzothiazole) (2-hydrazinobenzothiazole)

2.3. Procedure for the synthesis of Schiff base ligands (HMAB, HPAB and HVAB)

Various ligands were prepared by condensing 2-hydrazinobenzothiazole with respective aldehyde and ketone as follows.

2-hydrazinobenzothiazole (0.01 mol) in absolute ethanol (20 mL) was added to an ethanolic (20 mL) solution of o-hydroxyacetophenone/o-hydroxybenzophenone/o-vanillin (0.01 mol), followed by addition of 2 drops of acetic acid therein. The resulting solution was heated for 3 h on a water bath. The coloured and clear solution was allowed to evaporate at room temperature and washed with diethyl ether and finally, recrystallized in ethanol. Some microcrystalline product was obtained. Unfortunately, we didn't find anyone of them suitable for diffraction.

2.4. Procedure for the synthesis of metal complexes

The hydrated metal (II) chloride (0.01 mol) in absolute ethanol (20 mL) was treated with ethanolic (20 mL) solution of Schiff base ligand (0.02 mol) in 1:2 M ratio. The pH of the resulting mixture was adjusted to 7.5 to 8.0 by adding solid NaOH. It was refluxed for about 2 h leading to the formation of precipitate. Then filtered, washed with ether and finally dried in vacuo over fused $CaCl_2$. The re-crystallization process is carried out at room temperature for few days with a mixture of solvents by slow evaporation. But unfortunately, we didn't find crystals suitable for diffraction.

Scheme of the reaction for the formation of complexes:

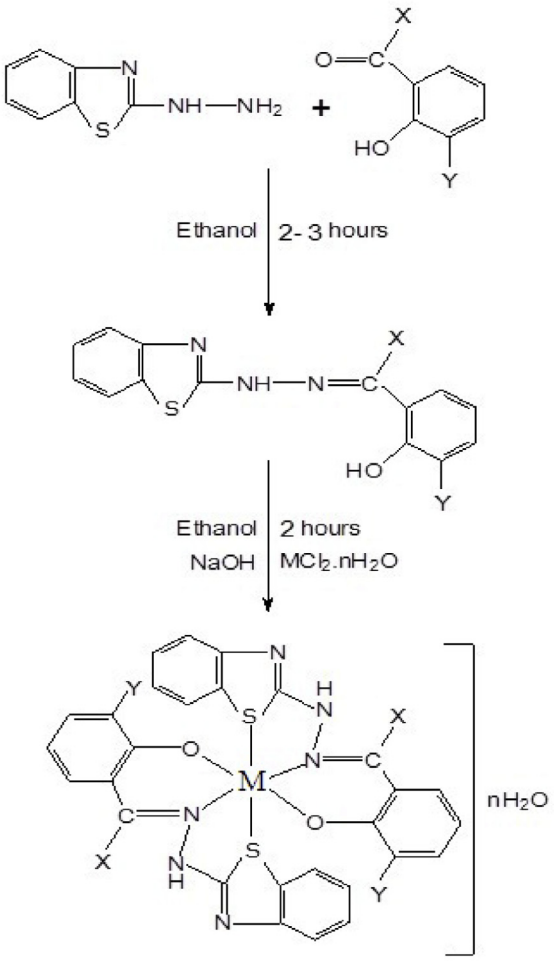

M= Co (II), Ni (II), Cu (II) and Zn (II)

X = -H, $-CH_3$, $-C_6H_5$, Y = -H, $-OCH_3$,

n = 1 or 2

2.5. Analysis and physical measurements

The metal contents were determined gravimetrically [16]. Conductivity measurements were recorded using Toshniwal Conductivity Bridge (model CL-01-06). The room temperature magnetic susceptibility measurements were recorded by Guoy method. Microanalyses (C, H, N) were executed by using a MLW-CHN micro analyzer. The electronic spectra were obtained in DMSO from a Perkin-Elmer spectrophotometer. FTIR spectra as KBr pellets were recorded using Varian FTIR spectrophotometer, Australia. Thermogravimetric analysis was executed by using Netzch-429 thermo analyzer. ^1H NMR and C^{13} NMR spectra were collected from JEOL

GSX-400 model equipment in DMSO-d_6 medium. The ESR spectra were obtained from a varian E-112 ESR Spectrophotometer.

2.6. DFT studies

Schiff base ligands and its Cu^{II} and Zn^{II} complexes were optimized and analyze with Gauss View 5.0.8 programme [17]. The GAUSSIAN 03 programme platforms [18–24] were used for DFT calculations with LANL2DZ basic set. The Cu(II) and Zn(II) metal were use LANL2DZ basic set in gas phase and 6-31 G (d, p) basic set are used for rest of the atoms.

2.7. Molecular docking studies

Molecular docking is one of the important drug design tools to understand the binding pattern of investigated compounds toward target proteins CYP121 and Cytochrome P450 14 alpha-sterol demethylase (CYP51) from *Mycobacterium tuberculosis*. The docking study was analyzed by using AutoDock Vina software. Crystallographic structures of CYP121 (PDB: 2IJ7) and CYP51 (PDB: 1EA1) proteins [25] were brought from Protein Data Bank (http://www.pdb.org). The proteins were freed from inbound ligand (fluconazole) by Discovery Studio 3.5 Visualizer [26]. Then polar hydrogen atoms and Kolhman charges were added to the proteins by using the AutoDock Tools (ADT). The grid box was selected for proteins centred at the crystal structure of the corresponding inbound ligand. The grid dimensions were kept with a spacing of 1 Å. On the other hand, the ligand structures were prepared by adding polar hydrogen atoms, Gasteiger partial charges, and the torsions were allowed to rotate. The docked poses were visualized by using the PyMOL software [27].

2.8. Antifungal assay

The *in vitro* antifungal activities of the compounds were examined at 100, 150, 200 μg mL^{-1} concentrations by Agar Well Diffusion Technique [28] against *A. flavus* and *A. niger*. Solutions of the compounds in DMSO were plated onto the cultured agar medium and incubated for a period of 48 h at 28°C. The results were measured in terms of zone of inhibition (in cm). Negative control used was DMSO. For comparison, the standard drug gentamycin is also screened under identical conditions.

3. Results and discussion

The analytical data and physical properties of the compounds are listed in Table-1, which are in good agreement with the calculated values. These reported metal complexes are coloured, non hygroscopic in nature and soluble in DMSO and DMF.

3.1. IR spectra

The most significant changes in the IR spectra of the condensation products of 2-hydrazinobenzothiazole with o-hydroxy acetophenone, o-hydroxy benzophenone or o-vanillin is the disappearance of the $-NH_2$ stretching and bending vibration. A new band assignable to $\nu_{C=N}$ (azomethine) appears at ~1560 cm^{-1} resulting from condensation of the precursor with above aldehyde or ketones. Besides, all these ligands exhibit a broad and strong band in the region ~3300 cm^{-1} attributed to phenolic –OH stretching vibration [29].

In the metal complexes (Table 2), band at ~ 3300 cm^{-1} due to phenolic –OH stretching vibration disappears, there by indicating it's deprotonation and coordination to the metal ions through oxygen [30]. This is further supported by the hypsochromic shift of phenolic ν_{C-O} mode around ~1280 cm^{-1} of the free ligand by 10–20 cm^{-1} [31]. Moreover, the position of band due to ν_{N-H} and ν_{C-N} remain unaltered indicating non-involvement of imino nitrogen in coordination.

The characteristic bands at ~1540, ~1313 and ~845 cm^{-1} can tentatively be assigned to $\nu_{C=N}$ (cyclic), ν_{C-N} (cyclic) and ν_{C-S-C} mode of vibration respectively. In the spectra of complexes former two bands do not change, indicating nonparticipation of ring nitrogen atom in coordination. However the later band shifts to lower frequency by 10–20 cm^{-1} in all complexes showing coordination of ring sulphur to the metal ions. Besides this, the bands due to $\nu_{C=N}$ (azomethine) and ν_{N-N} vibration shift their position in the metal complexes. The former band shifts to lower frequency by 10–20 cm^{-1} in all complexes which implies coordination of a azomethine nitrogen atom [32,33]. Occurrence of ν_{N-N} band at higher frequency region suggest a reduction in repulsion between the lone pair of nitrogen atom due to electron drainage to metal ion as a result of coordination via azomethine nitrogen.

All the metal complexes have a pair of sharp bands with moderate intensity around ~550 and ~462 cm^{-1} attributed to ν_{M-N} and ν_{M-O} vibrations respectively. Besides these, the band appearing at ~2567 cm^{-1} in the IR spectra of the ligand HVAB may be assigned to stretching vibration of – OCH_3

Group [34]. The position of this band remains unchanged showing non-coordination of $-OCH_3$ group most probably due to steric reason. In addition, the IR spectra of all the complexes show the presence of lattice water which is further proved by thermal

Table 1
Analytical and physical data of the ligands and complexes.

Sl no	Compounds	Colours	Yields (%)	Λ^a_m	C Found (Calcd)	H Found (Calcd)	N Found (Calcd)	S Found (Calcd)	M Found (Calcd)
1	HMAB	Dark green	80	–	63.55 (63.60)	4.57 (4.59)	14.80 (14.84)	11.27 (11.31)	–
2	HPAB	Light brown	75	–	69.53 (69.56)	4.31 (4.35)	12.15 (12.17)	9.24 (9.27)	–
3	HVAB	Orange	70	–	60.16 (60.20)	4.32 (4.35)	14.01 (14.05)	10.67 (10.70)	–
4	$[Co(MAB)_2]H_2O$	Dark brown	61	12.37	56.13 (56.16)	3.70 (3.74)	13.08 (13.10)	9.95 (9.98)	9.17 (9.20)
5	$[Ni(MAB)_2]\ H_2O$	Leaf green	62	10.75	56.15 (56.20)	3.71 (3.75)	13.08 (13.11)	9.96 (9.99)	9.09 (9.13)
6	$[Cu(MAB)_2]\ 2H_2O$	Red	64	11.48	54.23 (54.25)	3.58 (3.61)	12.62 (12.66)	9.61 (9.64)	9.53 (9.57)
7	$[Zn(MAB)_2]\ H_2O$	Light yellow	62	14.21	55.60 (55.64)	3.68 (3.71)	12.94 (12.98)	9.87 (9.89)	10.01 (10.04)
8	$[Co(PAB)_2]\ H_2O$	Brick red	63	11.23	62.71 (62.74)	3.62 (3.66)	10.95 (10.98)	8.32 (8.36)	7.66 (7.71)
9	$[Ni(PAB)_2]H_2O$	Green	64	12.57	62.74 (62.78)	3.63 (3.66)	10.95 (10.98)	8.34 (8.37)	7.61 (7.65)
10	$[Cu(PAB)_2]\ 2H_2O$	Dark brown	60	10.33	60.91 (60.95)	3.52 (3.55)	10.61 (10.66)	8.08 (8.12)	8.02 (8.06)
11	$[Zn(PAB)_2]\ H_2O$	White	61	9.52	62.21 (62.25)	3.59 (3.63)	10.85 (10.89)	8.27 (8.32)	8.40 (8.43)
12	$[Co(VAB)_2]\ H_2O$	Pale yellow	62	7.23	53.46 (53.49)	3.52 (3.56)	12.44 (12.48)	9.45 (9.50)	8.72 (8.76)
13	$[Ni(VAB)_2]\ H_2O$	Brick red	61	10.17	53.50 (53.53)	3.53 (3.57)	12.45 (12.49)	9.48 (9.51)	8.65 (8.70)
14	$[Cu(VAB)_2]\ 2H_2O$	Pea green	61	8.18	51.72 (51.76)	3.41 (3.45)	12.02 (12.07)	9.18 (9.20)	9.09 (9.13)
15	$[Zn(VAB)_2]\ H_2O$	Sky blue	63	10.22	52.99 (53.02)	3.50 (3.53)	12.33 (12.37)	9.37 (9.42)	9.54 (9.57)

[a] $Ohm^{-1}\ cm^2\ mole^{-1}$.

Table 2
Infrared spectral data of the complexes (in cm^{-1}).

HMAB	$[Cu(MAB)_2]2H_2O$	HPAB	$[Co(PAB)_2]\ H_2O$	HVAB	$[Ni(VAB)_2]\ H_2O$	Assignments
_	3481	–	3485	–	3490	$\nu_{O\text{-}H}$(lattice water)
2875	2872	–	–	–	–	$\nu_{C\text{-}H}(-CH_3)$
_	–	–	–	2572	2569	$\nu(-OCH_3)$
1630	1630	1625	1627	1625	1625	$\nu_{C=C}$(cyclic)
1605	1602	1608	1606	1610	1607	$\delta_{N\text{-}H}$
1550	1537	1553	1535	1559	1540	$\nu_{C=N}$(azomethine)
1508	1505	1510	1513	1510	1512	$\nu_{C=N}$(cyclic)
_	1317	–	1300	–	1305	$\nu_{C\text{-}O}$
1272	1266	1275	1270	1270	1271	$\nu_{C\text{-}N}$(exocyclic)
1045	1038	1040	1030	1035	1022	$\nu_{N\text{-}N}$(exocyclic)
955–630	930–645	955–660	950–655	960–650	955–640	$\delta_{C\text{-}H}$(out of plane)
852	836	865	850	860	844	$\nu_{C\text{-}S\text{-}C}$
_	552	–	540	–	555	$\nu_{M\text{-}N}$
_	462	–	456	–	460	$\nu_{M\text{-}O}$

study. Hence the ligands act as monobasic tridentate donors coordinating through azomethine nitrogen, ring sulphur and deprotonated phenolic oxygen to yield metal complexes of the composition $ML_2.nH_2O$. The representative IR spectrum of $[Cu(MAB)_2\ 2H_2O]$ is shown in (Graph 1).

3.2. Thermal analysis

The metal complexes follow similar pattern of thermal decomposition. All the metal complexes lose water below 100 °Cindicating to be lattice water [35]. The anhydrous complexes again start decomposing rapidly around ~300 °C due to decomposition of organic constituents in the complexes. Decomposition continues up to ~700 °Cand produces their stable oxides. Thermal data of these complexes are enlisted in (Table 3). The thermal stability can be summarized as follows.

MAB complexes: Co (II) < Ni (II) < Zn (II) < Cu (II)
PAB complexes: Ni (II) < Co (II) < Cu (II) < Zn (II)
VAB complexes: Ni (II) < Co (II) < Zn (II) < Cu (II)

3.3. Electronic spectra and magnetic properties

The electronic spectra of Co(II) complexes in DMSO contain two main bands, a very broad and a strong band around ~10,500 cm^{-1} (952 nm) and ~22,000 cm^{-1} (454 nm) respectively. The former band can be attributed to $^4T_{1g}(F) \rightarrow {}^4T_{2g}(F)$ (ν_1) and the later to $^4T_{1g}(F) \rightarrow {}^4T_{1g}$ (P) (ν_3) transitions respectively. Besides these the spectra also has two shoulders at ~19,500–21,500 cm^{-1} (512-465 nm) and ~16,000–17,000 cm^{-1} (625-590 nm) region. The magnetic moment values of Co(II) complexes lie in the range normally seen for octahedral Co(II) species.

The electronic spectra of Ni(II) complexes are found to possess a split band system followed by two main bands. The main bands observed at ~15,000 cm^{-1} (667 nm) and ~24,500 cm^{-1} (417 nm) may safely be attributed to $^3A_{2g}(F) \rightarrow {}^3T_{2g}(F)$,($\nu_2$) and $^3A_{2g}(F) \rightarrow {}^3T_{1g}(P)$ (ν_3) transitions respectively under octahedral symmetry. However, the value of transition energy ratio ν_3/ν_2 observed for these complexes are lower than the usual range (~1.7) for octahedral Ni(II) species. This decrease in value might be due to some distortion from octahedral geometry. The split band at ~8600 cm^{-1} (1163 nm) and ~10,200 cm^{-1} (980 nm) might be due to splitting of ν_1 band under D_{4h} symmetry and can be attributed to $^3B_{1g} \rightarrow {}^3E_g$ and $^3B_{1g} \rightarrow {}^3B_{2g}$ transitions respectively. The amount of splitting of ν_1 band is taken as a measure of degree of distortion. The μ_{eff} values of Ni(II) complexes lie in the range expected for either octahedral or pseudo-octahedral Ni(II) species.

The electronic spectra of all these Cu(II) complexes (Graph 2) are similar in nature. Here the spectra is characterized by two bands at ~14,200 cm^{-1} (704 nm) and ~16,810 cm^{-1} (594 nm) which may be attributed to $^2B_{1g} \rightarrow {}^2B_{2g}$ (ν_2) and $^2B_{1g} \rightarrow {}^2E_g$ (ν_3) transitions, suggesting there by a distorted octahedral geometry for these complexes like the previous case. In this case also the band due to $^2B_{1g} \rightarrow {}^2A_{1g}$ is not observed most probably due to superimposition by ν_2 band owing to its broadness. Like our previous discussion here also no band occurs below ~10,000 cm^{-1} there by ruling out possibility of tetrahedral or pseudo-tetrahedral geometry. The μ_{eff}

Table 3
Important features of thermogravimetric analysis (TGA).

Complexes	Total wt. for TG (mg)	Temp. range of Water loss (°C)	% of water loss		Decomposition temperature (°C)	% of residue		Composition of the residue
			Found	Calc.		Found	Calc.	
4	19.8	40–100	2.78	2.81	240	11.66	11.70	CoO
5	17.7	50–110	2.77	2.81	260	11.60	11.63	NiO
6	21.5	50–110	5.38	5.42	285	11.93	11.98	CuO
7	11.4	45–100	2.73	2.78	235	12.48	12.52	ZnO
8	20.8	50–100	2.32	2.35	235	9.75	9.80	CoO
9	15.6	50–100	2.31	2.35	250	9.70	9.74	NiO
10	16.3	40–110	4.53	4.57	270	10.05	10.09	CuO
11	12.5	50–100	2.30	2.33	260	10.45	10.50	ZnO
12	14.1	50–115	2.62	2.67	230	11.11	11.14	CoO
13	13.8	50–100	2.64	2.68	235	11.04	11.08	NiO
14	17.5	40–100	5.15	5.17	255	11.40	11.43	CuO
15	18.7	45–95	2.61	2.65	265	11.89	11.93	ZnO

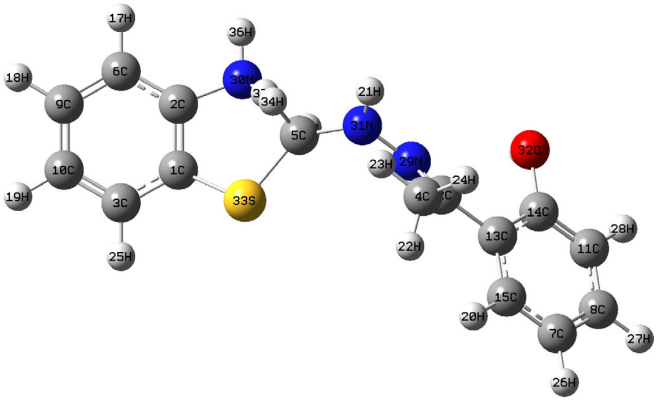

Fig. 1. Optimized geometry of the ligand HMAB (L_1).

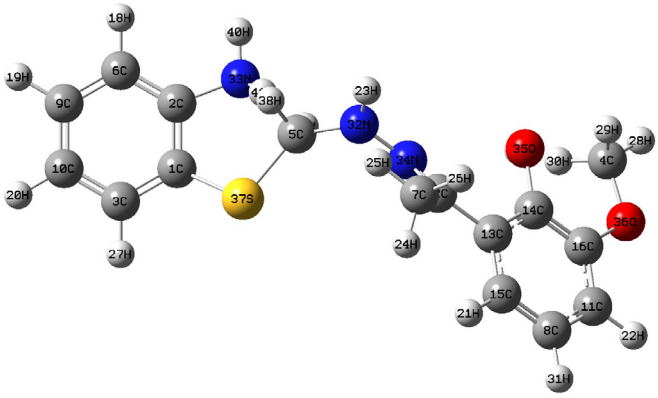

Fig. 3. Optimized geometry of the ligand HVAB (L_3).

values of Cu(II) complexes lie in the range 1.79–1.90 B.M. which is normal for hexa coordinated Cu(II) complexes.

3.4. NMR spectra

The ^{1}H NMR spectrum of the compounds display a multiplet in the region δ 7.2–7.9 ppm corresponding to 8/13/7 aromatic protons, while the signals due to exocyclic −NH−N = proton appear at δ 9.1 ppm. A signal is also observed at δ 2.4 ppm due to $-CH_3$ protons in case of ligand HMAB. In addition, signals due to azomethine (-N=CH−) and $-OCH_3$ protons observed at δ 8.7 ppm and δ 4.3 ppm respectively. The disappearance of the phenolic OH proton signal and the downfield signal due to the azomethine protons, indicate the co-ordination of above groups to the metal ion. This was also confirmed from IR study. The ^{13}C NMR spectrum of the synthesized compounds explains the electronic environment of different kind of carbon atoms present. In the ^{13}C NMR spectrum, signals appeared in the region 105.4 to 153.2 are due to aromatic carbons. The signals at 176.4, 169.1 and 18.3 are assigned to C=N (azomethine), C=N (benzothiazole moiety) and CH_3 respectively. The representative ^{1}H NMR and ^{13}C NMR spectra of [Zn(MAB)$_2$ H_2O] are shown in (Graph 3 and Graph 4) respectively.

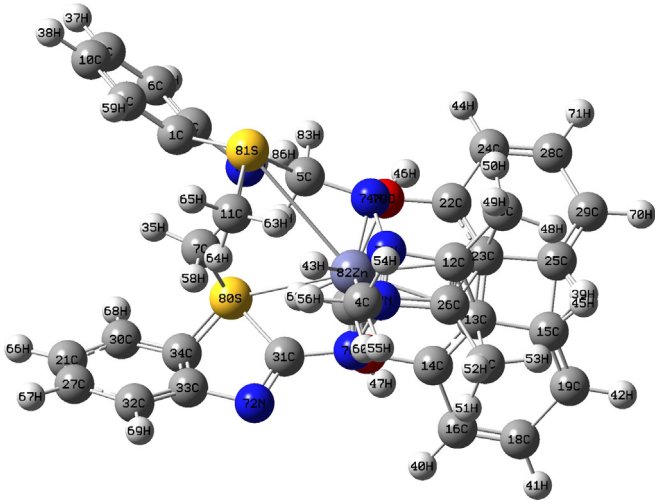

Fig. 4. Optimized geometry of the complex [Zn(MAB)$_2$] H_2O.

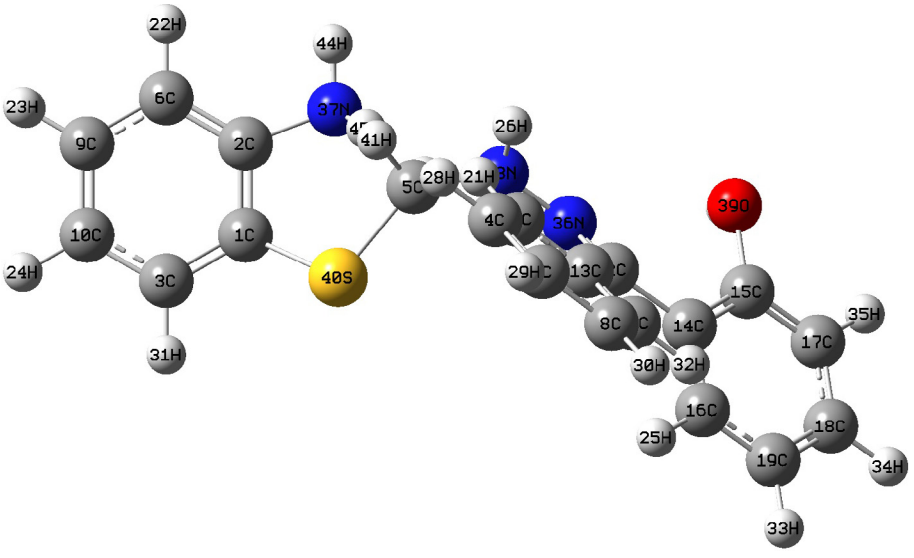

Fig. 2. Optimized geometry of the ligand HPAB (L_2).

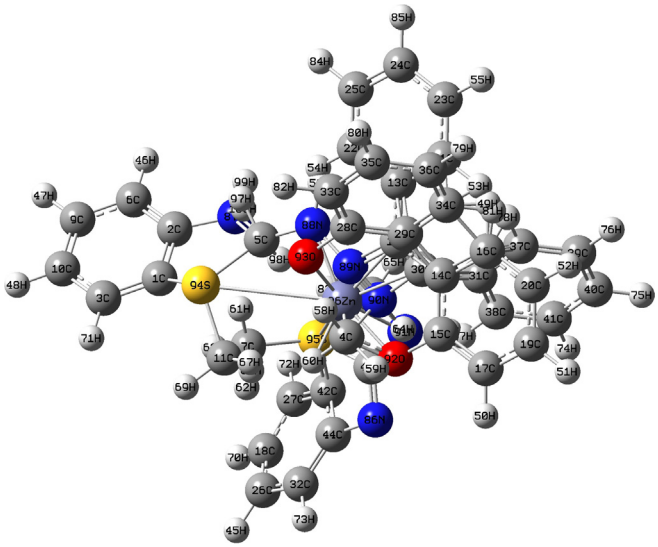

Fig. 5. Optimized geometry of the complex $[Zn(PAB)_2]$ H_2O.

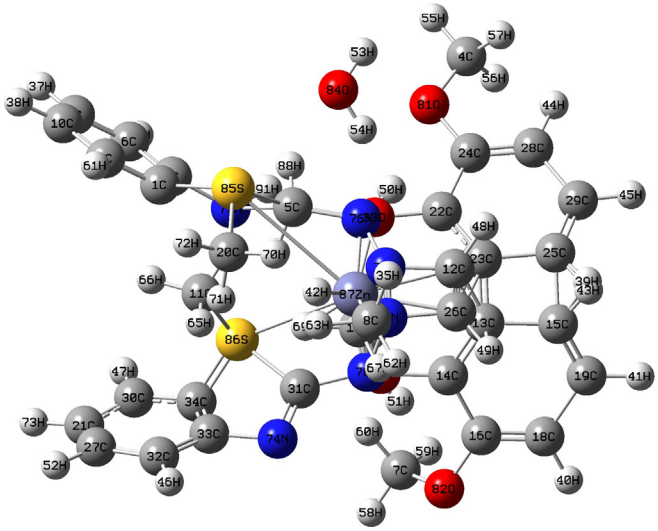

Fig. 6. Optimized geometry of the complex $[Zn(VAB)_2]$ H_2O.

3.5. ESR spectra

The ESR spectra of Cu(II) complexes were recorded in DMSO at 300 K, which exhibits a well resolved four line spectrum for mononuclear nature. There was no features characteristic for a binuclear complex. This is also supported by the magnetic moment values. The spin Hamiltonian parameters were calculated from the spectrum. The observed order ($g_{11} = 2.26 > g_{\perp} = 2.07 > 2.0023$) indicates that the complex has octahedral geometry [36]. This also suggests that the unpaired electron exists in d^{22}_{x-y} orbital [37], as evident from exchange interaction term G ($G = 3.8 < 4.0$). Here, $g_{11} < 2.3$ explains the covalent nature of the M→L bonding [38]. The covalency parameter α^2 is also calculated, which suggests the covalent nature of the copper complexes (Graph 5).

3.6. Powder X-ray diffraction

The X-ray diffraction (powder pattern) for $[Co(MAB)_2]$ H_2O complex is analyzed through Phillips X'Pert High score software. The prominent diffraction peaks were indexed and analyzed by using LSUCRPC programme package [39] (Graph 6). The lattice constant such as ($a = 9.566$ Å, $b = 11.143$ Å, $c = 6.751$ Å, $\alpha = 104.98^0$, $\beta = 101.65^0$, $\gamma = 75.31^0$, Volume = 665.23, Density = 1.688 g/cm^3. For the confirmation of diffraction pattern a comparison was made between detected and evaluated 2θ values which are supports from the figure of merit value (7.3) as proposed by de-Woulff [40]. Standard floatation techniques was used to determine the density (ρ) of the cobalt complex. The number of unit cell (n) is evaluated from the following equation

$$\mathbf{n} = \frac{\rho NV}{M}$$

The number of unit cell 'n' is establish to be 1.5 that concur well with the proposed triclinic crystal shape of the cobalt complex. Average particle dimension of the cobalt complex can be calculated by using the following Debye Scherrer equation

$$\boldsymbol{D} = \boldsymbol{K}\lambda/\beta\ \mathbf{Cos}\ \theta$$

After calculation it is found that the particle size of $[Co(MAB)_2]$ H_2O complex is 5.6 nm [41].

3.7. Molecular modelling studies (geometrical optimization and DFT computation)

Three ligands HMAB (L_1), HPAB (L_2), HVAB (L_3) and its Zn complexes (Figs. 1–6) were optimized with the help of B3LYP/6-31G (d, p) and B3LYP/LANL2DZ basic sets for there configurational stable geometry. The observation have been found for the bond lengths and the bond angles of ligands varies in comparison with metal complexes mentioned in (Table 4 and Table 5) that indicate the mode of bonding between ligand donor atoms with the metal ions [42,43].

The calculation of dipole moment and single point energy value of the ligands HMAB (L_1), HPAB (L_2), HVAB (L_3) and $[Zn(MAB)_2]$ H_2O, $[Zn(PAB)_2]$ H_2O $[Zn(VAB)_2]$ H_2O, $[Cu(MAB)_2]$ $2H_2O$, $[Cu(PAB)_2]$ $2H_2O$, $[Cu(VAB)_2]$ $2H_2O$ complexes are evaluated by DFT/B3LYP 6-

Table 4
Specified bond length (Å) and bond angle (°) of the ligands.

HMAB (L_1) B3LYP/6.31G (d, p)		HPAB (L_2) B3LYP/6.31G (d, p)		HVAB (L_3) B3LYP/6.31G (d, p)	
Bond length (Å)	Bond Angle (°)	Bond length (Å)	Bond Angle (°)	Bond length (Å)	Bond Angle (°)
C2–S20 (1.789)	C6–C2–S20 (129.004)	C2–S40 (1.789)	C1–C2–S40 (129.004)	C2–S34 (1.789)	C6–C2–S34 (129.004)
C5–S20 (1.856)	C2–S20–C5 (81.507)	C5–S40 (1.857)	C2–S40–C5 (81.449)	C5–S34 (1.856)	C2–S34–C5 (81.514)
C5–N16 (1.244)	N16–C5–S20 (120.350)	C5–N36 (1.243)	S40–C5–N38 (118.222)	C5–N31 (1.244)	S34–C5–N31 (120.347)
C5–N18 (1.446)	C5–N18–N17 (120.003)	C5–N38 (1.446)	N38–N37–C12 (120.047)	C5–N29 (1.446)	S34–C5–N29 (118.225)
N17–N18 (1.351)	N17–N18–C12 (120.029)	N37–N38 (1.351)	N37–C12–C14 (119.985)	N29–N30 (1.351)	C5–N29–N30 (119.998)
N17–C12 (1.243)	N17–C12–C4 (119.967)	N37–C12 (1.243)	C14–C20–O39 (119.976)	N30–C12 (1.243)	N29–N30–C12 (120.027)
C14–O19 (1.409)		C20–O39 (1.409)	C8–C20–O39 (120.001)	C14–O32 (1.409)	C13–C14–O32 (119.950)
					C11–C14–O32 (120.036)

Table 5
Specified bond length (Å) and bond angle (°) of the complexes.

[Zn(MAB)$_2$ H$_2$O] (L_1) B3LYP/6.31G (d, p)		[Zn(PAB)$_2$ H$_2$O] (L_2) B3LYP/6.31G (d, p)		[Zn(VAB)$_2$ H$_2$O] (L_3) B3LYP/6.31G (d, p)	
Bond length (Å)	Bond Angle (°)	Bond length (Å)	Bond Angle (°)	Bond length (Å)	Bond Angle (°)
C34–S80 (1.567)	C30–C34–S80 (120.691)	C1–S94 (1.790)	C2–C1–S94 (111.011)	C1–S85 (1.930)	C2–C1–S85 (106.533)
C31–S80 (1.789)	C31–S280–C34 (88.924)	C5–S94 (1.789)	C1–S94–C5 (103.975)	C5–S85 (1.482)	C1–S85–C5 (93.048)
S80–Zn82 (2.832)	N72–C31–S80 (110.982)	S94–Zn96 (3.363)	N87–C5–S94 (93.050)	S85–Zn87 (2.628)	N76–C5–S85 (105.398)
C26–N77 (1.446)	C31–N76–N77 (120.002)	C5–N87 (1.938)	C5–N88–N89 (120.032)	C5–N76 (1.282)	C5–N75–N76 (139.381)
N77–Zn82 (0.858)	N76–N77–C26 (109.511)	N88–Zn96 (1.897)	N88–N89–C12 (109.493)	N76–Zn87 (1.756)	N76–N77–C12 (99.621)
N76–N77 (1.351)	N77–C26–C17 (119.988)	N88–N89 (1.349)	N89–C12–C14 (120.034)	N76–N77 (2.157)	N77–C12–C23 (124.868)
O78–Zn82 (1.889)	Zn82–O78–C14 (109.557)	O93–Zn96 (1.889)	Zn96–O93–C28 (109.521)	O83–Zn87 (2.083)	Zn87–O83–C22 (104.393)
C14–O80 (1.398)		C28–O93 (1.410)		C22–O83 (1.358)	

Table 6
Energetic properties of the ligands and its copper and zinc complexes calculated by DFT/B3LYP 6.31G (d, P) and DFT/B3LYP LANL2DZ basic sets.

Compound	Single point energy in kcal/mol		Dipole moment (D)	
	DFT/B3LYP 6.31G (d, P)	DFT/B3LYP LANL2DZ	DFT/B3LYP 6.31G (d, P)	DFT/B3LYP LANL2DZ
HMAB (L_1)	-7.6498×10^5	–	0.587	–
HPAB (L_2)	-8.8555×10^5	–	0.520	–
HVAB (L_3)	-8.3680×10^5	–	0.270	–
[Cu(MAB)$_2$] 2H$_2$O	-2.6336×10^5	-1.0432×10^5	1.821	1.732
[Zn(MAB)$_2$] H$_2$O	-2.7194×10^5	-1.3271×10^5	−1.364	−1.113
[Cu(PAB)$_2$] 2H$_2$O	-4.7519×10^5	-1.9768×10^5	1.235	1.117
[Zn(PAB)$_2$] H$_2$O	-5.8136×10^5	-2.0237×10^5	−1.781	−1.005
[Cu(VAB)$_2$] 2H$_2$O	-3.3478×10^5	-1.8113×10^5	1.201	1.034
[Zn(VAB)$_2$] H$_2$O	-3.5619×10^5	-2.0031×10^5	−1.667	−0.978

Table 7
QSAR Calculation for optimized ligands.

Function	Ligand HL_1	Ligand HL_2	Ligand HL_3
Surface area (Approx) (Å^2)	395.80	431.05	429.68
Surface area (Grid) (Å^2)	516.61	596.14	543.66
Volume (Å^3)	830.28	985.07	888.94
Hydration energy (Kcal/mole)	−11.83	−11.60	−12.51
Log P	3.83	5.07	3.59
Refractivity (Å^3)	26.26	24.99	32.68
Polarizability (Å^3)	31.68	39.51	34.15
Mass (amu)	283.35	345.42	313.37
Total energy (kcal/mol)	−67838.69903	−82190.90694	−78049.44403
Binding energy (kcal/mol)	−3636.021773	−4559.901623	−4006.222971
Heat of formation (kcal/mol)	69.6132273	104.3873772	34.06502904
Electronic energy (kcal/mol)	−453632.6312	−627111.863	−550612.2171
Nuclear energy (kcal/mol)	385793.9322	544920.9561	472562.7731
Free energy (kcal/mol)	−67838.7	−82190.9	−78049.4

31G (d, p) and DFT/B3LYP LANL2DZ basic sets (Table 6). In comparison among all three ligands single point energy of HPAB (L_2) is possesses less energy which indicates greater stability. Similarly comparison made with metal complexes of all the ligands [Cu(PAB)$_2$] 2H$_2$O and [Zn(PAB)$_2$] H$_2$O complexes possesses less energy and having greater stability [44]. In both the basic set of all the Cu complexes possesses higher dipole moment value in comparison with all the Zn complexes. This clearly indicates all the Cu complexes have stronger dipole-dipole interaction.

3.8. QSAR studies

The QSAR study of the ligands was made by using HyperChem Professional 8.0.3 software. All the structures of the ligands are optimized by applying molecular mechanics force field (MM^+) followed by semi-empirical PM3 methods. The minimization of energy was done by applying Fletcher-Reeves conjugate gradient algorithm. The calculated Partition coefficient log P of the ligands ($HL_1 = 3.83$, $HL_2 = 5.07$ and $HL_3 = 3.59$) respectively. The log P values explain the biological effectiveness of the ligands. The major

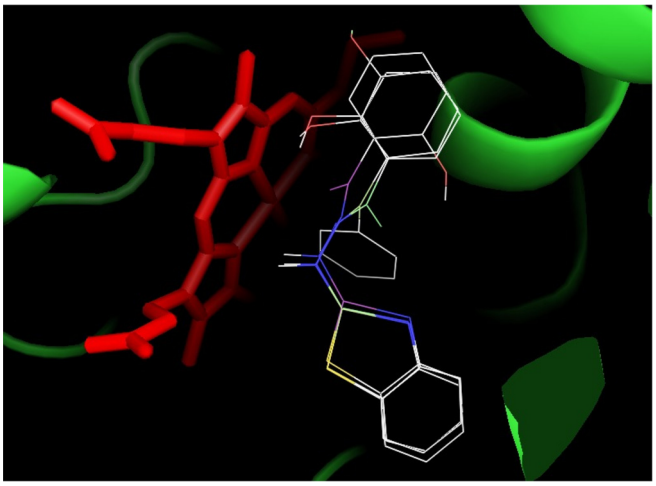

Fig. 7. Docking conformation for the compounds (L1-L3, in wire form) at the CYP51 (PDB: 1EA1) binding site (Protoporphyrin molecule is shown in red stick).

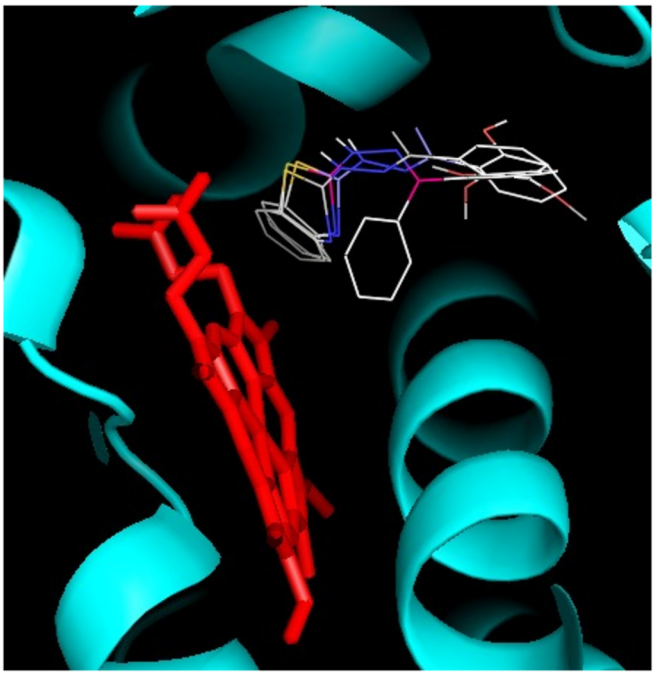

Fig. 8. Docking conformation for the compounds (L1-L3, in wire form) at the CYP121 (PDB:2IJ7) binding site (Protoporphyrin molecule is shown in red stick).

role is the permeability of the used compounds into the cell membrane [45]. Other essential parameters also calculated after completion of optimization (Table 7).

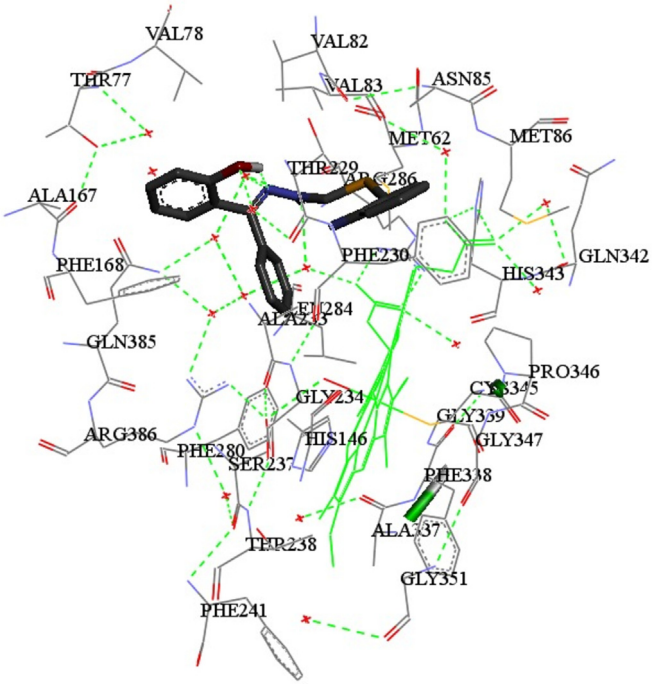

Fig. 10. CYP121 (PDB: 2IJ7) and ligand (L2) interactions: The binding residues and hydrogen bonding are represented as constructed in Discovery Studio Visualizer 3.5 (Accelrys, Biovia, USA) (Protoporphyrin molecule is shown in green wire).

3.9. Molecular docking studies

To identify how these molecules (L1, L2 and L3) can bind to CYP121 (PDB: 2IJ7) and CYP51 (PDB: 1EA1) proteins, molecular

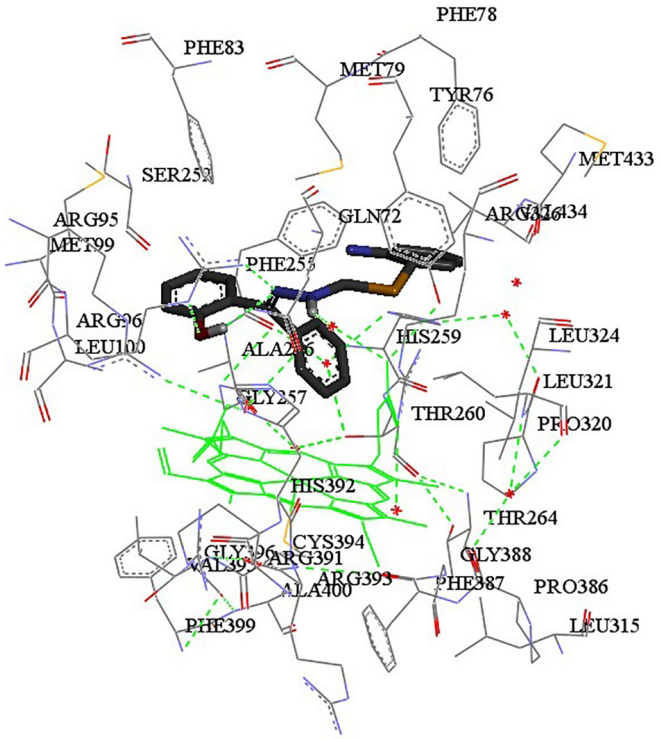

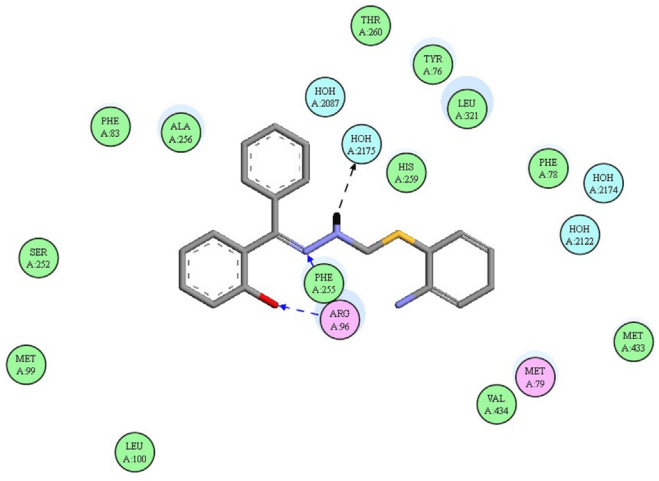

Fig. 9. a)CYP51 (PDB: 1EA1) and ligand (L2) 3D-interactions: The binding residues and hydrogen bonding are represented as constructed in Discovery Studio Visualizer 3.5 (Accelrys, Biovia, USA) (Protoporphyrin molecule is shown in green wire). b). CYP51 (PDB: 1EA1) and ligand (L2) 2D-interactions: The binding residues and hydrogen bondings are represented as constructed in Discovery Studio Visualizer 3.5 (Accelrys, Biovia, USA) (Protoporphyrin molecule is shown in green wire).

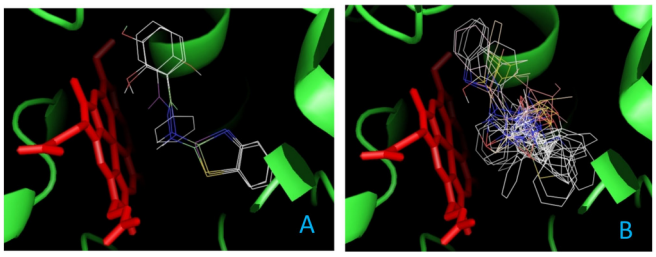

Fig. 11. Comparison of (A) L series ligands (L1, L2 and L3 in wire form) and (B) L2 in complexed with various ions (Cu, Co, Ni, Zn) with CYP51 (PDB: 1EA1). (Protoporphyrin molecule is shown in red stick).

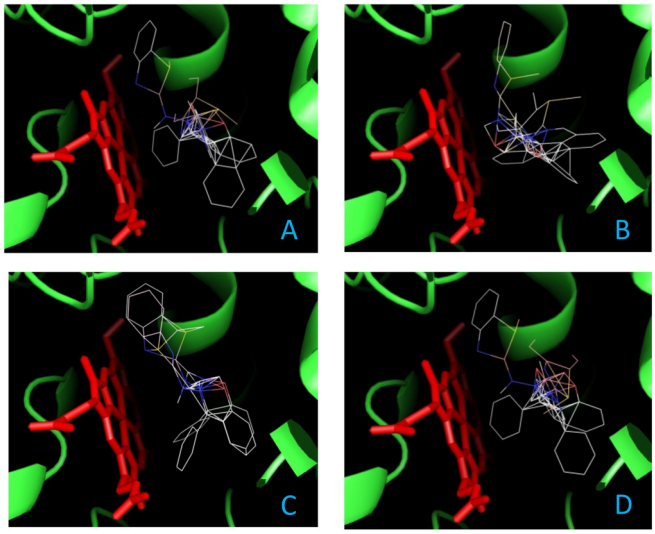

Fig. 12. CYP51 (PDB: 0/11EA1) and ligand complex (A) L2-Co, (B) L2-Cu, (A) L2-Ni, (B) L2-Zn interactions: (Protoporphyrin molecule is shown in green stick).

docking studies were carried out (Fig. 7 and Fig. 8). The docking protocol verified by re-docking the fluconazole into the active site of CYP121 (PDB: 2IJ7) and CYP51 (PDB: 1EA1) proteins. From the docking study, it was found that the ligand L2 shows the best affinity towards both of the proteins [46]. An overview of the receptor–inhibitor binding interaction is shown in Fig. 9(a) and (b) and Fig. 10. Further, the L2 in complexed with various ions (Cu, Co, Ni, Zn) were docked to understand the binding with CYP51 (PDB: 1EA1) (Figs. 11 and 12).

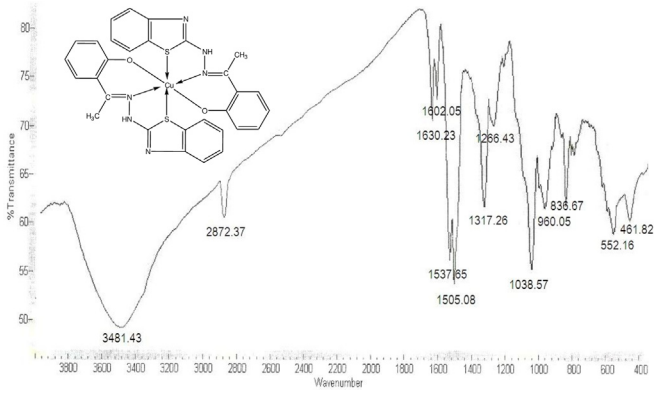

Graph 1. Infrared spectrum of $[Cu(MAB)_2]\ 2H_2O$.

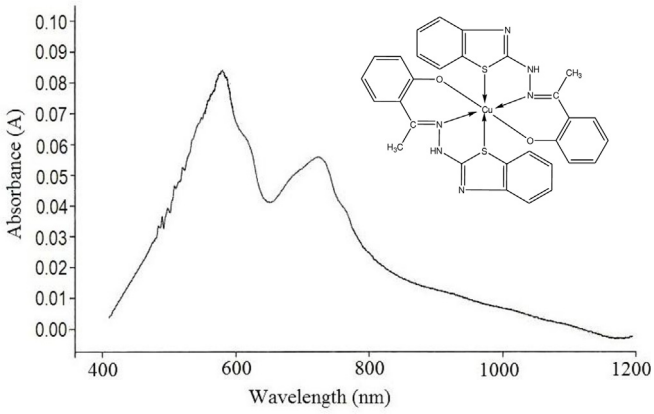

Graph 2. Electronic spectrum of $[Cu(MAB)_2]\ 2H_2O$.

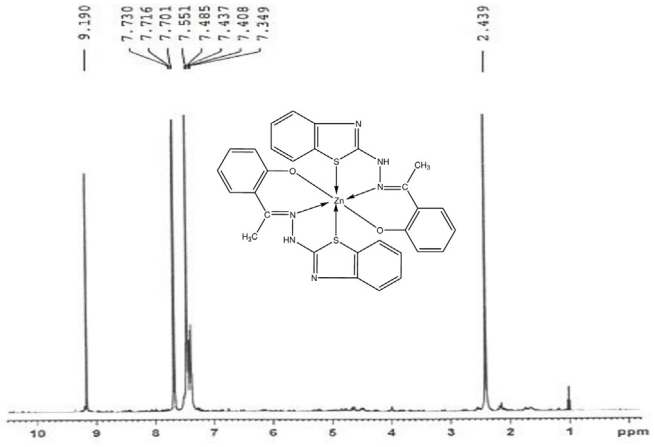

Graph 3. ^1H NMR spectrum of $[Zn(MAB)_2]\ H_2O$.

3.10. Antifungal activity

The *in vitro* antifungal activities of these compounds were examined at different concentrations by using Agar Well Diffusion Technique. The results of the study are given in (Table 8). It is observed that the metal complexes exhibit greater activity than the free ligands. This may be explained on the basis of chelation theory. It is also observed that, the activities of the synthesized metal complexes increase with increase in the concentration of the test solution. It is because the concentration plays a vital role in

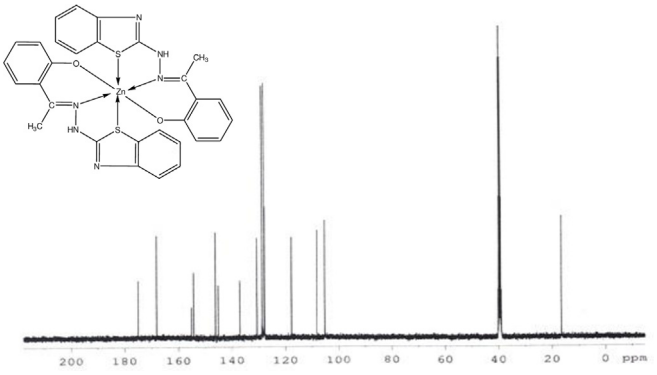

Graph 4. ^{13}C NMR spectrum of $[Zn(MAB)_2]\ H_2O$.

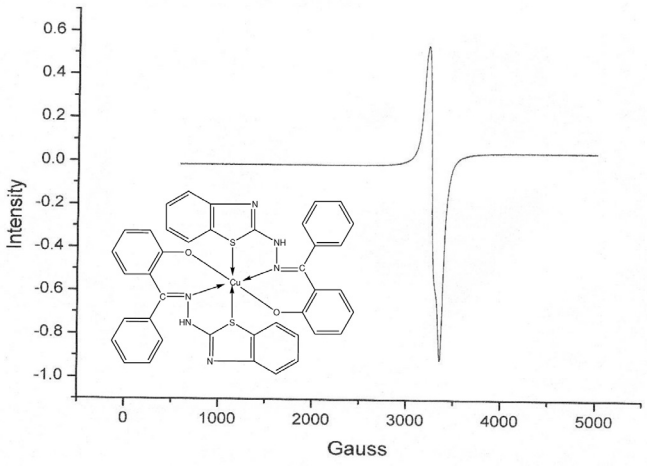

Graph 5. ESR spectrum of $[Cu(PAB)_2]$ $2H_2O$.

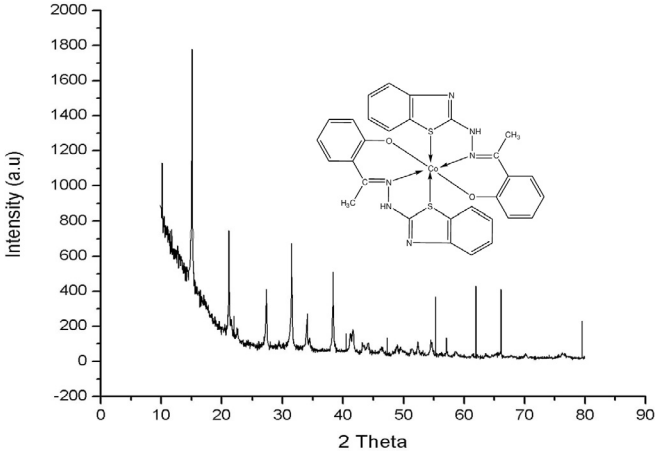

Graph 6. XRD graph of $[Co(MAB)_2]$ H_2O.

increasing the degree of inhibition of antifungal growth. In addition, many other factors like nature of the ligand, solubility, dipole moment, conductivity and geometry may be responsible for the higher activity [47,48]. The comparative antifungal activities of

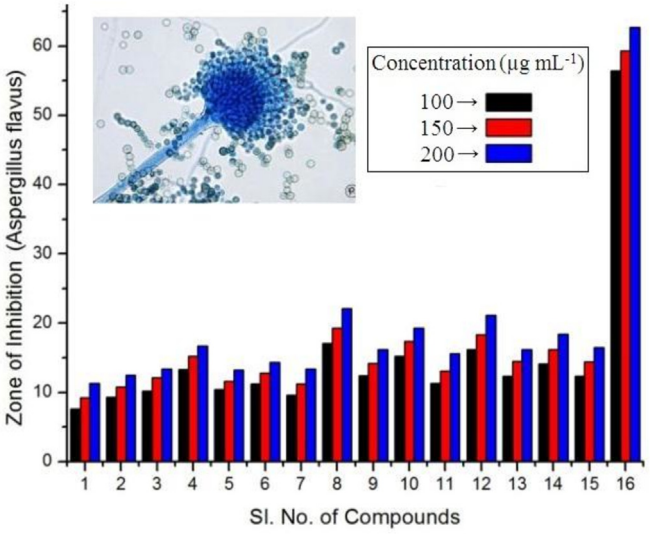

Graph 7. Effect of the ligands and complexes on the growth of *Aspergillus flavous*.

complexes with HMAB, HPAB and HVAB against two stains of fungi such as *A. flavus and A. niger* are shown in (Graph 7 and Graph 8).

4. Conclusion

The present study revealed that all these metal complexes are neutral in nature which is evident from their extremely low values of conductivity. All the metal complexes contain water molecules in their lattice, which certainly do not participate in coordination to the central metal ions as indicated from their thermal behavior. They are removed at a much lower temperature than the coordinated molecules. This is further corroborated from IR spectral investigations. The octahedral geometry of all the complexes are established with tridentate chelation of ligand. From the powder XRD pattern shows that the cobalt complex is triclinic crystal system. The molecular modelling study supports experimental findings of the bonding sites of the ligands, symmetry and stability of the complexes. The QSAR study of the ligands shows all the functional parameters of ligand HPAB is grater, so it is more potent among all the ligands. Molecular docking study was also carried out to explain the binding pattern of reported compounds toward target proteins CYP121 and CYP51. The study revealed that the

Table 8
Antifungal activities of the synthesized compounds (zone of inhibition in μg mL^{-1}).

Sl. No.	Compounds	*Aspergillus flavus*			*Aspergillus niger*		
		100 A (Black)	150 B (Red)	200C (Blue)	100 A (Black)	150 B (Red)	200C (Blue)
1	HMAB	7.6	9.2	11.3	9.4	10.8	12.3
2	HPAB	9.3	10.8	12.5	11.2	12.7	14.2
3	HVAB	10.2	12.1	13.4	13.5	15.1	16.6
4	$[Co(MAB)_2]H_2O$	13.3	15.2	16.7	14.4	16.3	18.2
5	$[Ni(MAB)_2]$ H_2O	10.4	11.6	13.2	12.1	14.2	16.3
6	$[Cu(MAB)_2]$ $2H_2O$	11.2	12.8	14.3	13.4	15.2	17.4
7	$[Zn(MAB)_2]$ H_2O	9.6	11.2	13.4	10.3	11.8	14.2
8	$[Co(PAB)_2]$ H_2O	17.1	19.3	22.1	16.2	18.5	21.1
9	$[Ni(PAB)_2]H_2O$	12.4	14.2	16.2	13.3	15.4	17.3
10	$[Cu(PAB)_2]$ $2H_2O$	15.2	17.4	19.3	15.6	17.8	20.1
11	$[Zn(PAB)_2]$ H_2O	11.3	13.1	15.6	12.2	14.3	16.2
12	$[Co(VAB)_2]$ H_2O	16.2	18.3	21.1	19.3	21.2	23.3
13	$[Ni(VAB)_2]$ H_2O	12.3	14.5	16.2	15.4	17.3	20.2
14	$[Cu(VAB)_2]$ $2H_2O$	14.1	16.2	18.4	17.1	19.2	21.4
15	$[Zn(VAB)_2]$ H_2O	12.3	14.4	16.5	14.4	16.2	18.3
16	Gentamycin (std.)	56.4	59.3	62.7	52.2	56.5	61.1

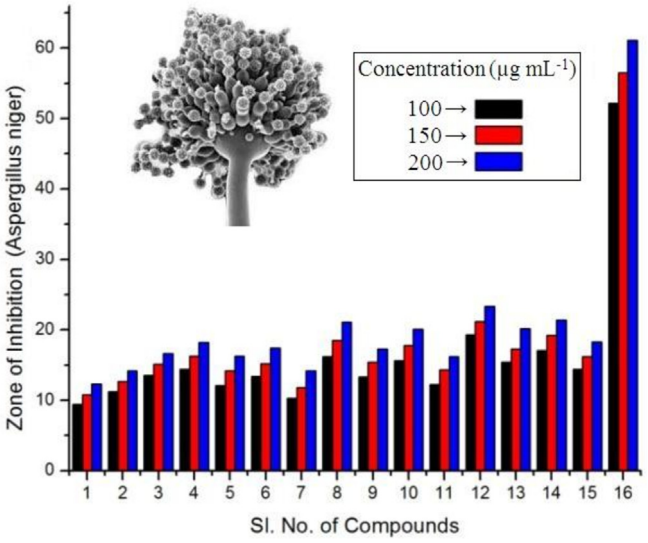

Graph 8. Effect of the ligands and complexes on the growth of *Aspergillus niger*.

ligand L_2 shows the best affinity towards both of the proteins. Furthermore, the metal complexes have greater antifungal activity as compared to the free ligands. This may be explained due to enhanced lipophilic property of the central metal ion as a result of chelation with the ligand moieties. Hence, this study will help the researchers to develop new antifungal agents with higher potency.

Acknowledgement

The authors (RKM & AKS) are grateful to the Principal, Government College of Engineering, Keonjhar for providing necessary facilities and support. The authors are also thankful to Sk. Abdul Amin, Natural Science Laboratory, Department of Pharmaceutical Technology, Jadavpur University, Kolkata (WB), for doing the molecular docking study.

References

[1] R.K. Mohapatra, M. Dash, U.K. Mishra, A. Mahapatra, D.C. Dash, Synth. React. Inorg. Metal-Org. Nano-Metal Chem. 44 (2014) 642–648.
[2] R.K. Mohapatra, U.K. Mishra, S.K. Mishra, A. Mahapatra, D.C. Dash, J. Kor. Chem. Soc. 55 (6) (2011) 926–931.
[3] R.M. Kumbhare, T.L. Dadmal, R. Pamanji, U.B. Kosurkar, L.R. Velatooru, K. Appalanaidu, Y.K. Rao, J.V. Rao, Med. Chem. Res. 23 (2014) 4404–4413.
[4] V.S. Padalkar, B.N. Borse, V.D. Gupta, K.R. Phatangare, V.S. Patil, P.G. Umape, N. Sekar, Arabian J. Chem. 9 (2016) S1125–S1130.
[5] K. Sampath, S. Sathiyaraj, C. Jayabalakrishnan, Med. Chem. Res. 23 (2) (2014) 958–968.
[6] B.N. Amit, R.V. Kamath, G.B. Khadse, Indian J. Heterocycl. Chem. 9 (2000) 309–310.
[7] L. Racane, S.K. Pavelic, R. Nhili, S. Depauw, C. Paul-Constant, I. Ratkaj, M.-H. David-Cordonnier, K. Pavelic, V. Tralic-Kulenovic, G. Karminski-Zamola, Eur. J. Med. Chem. 63 (2013) 882–891.
[8] A. Aboelmagd, I.A.I. Ali, E.M.S. Salem, M. Abdel-Razik, Eur. J. Med. Chem. 60 (2013) 503–511.
[9] V. Pejchal, M. Pejchalova, Z. Ruzickova, Med. Chem. Res. 24 (2015) 3660–3670.
[10] L. Racane, V. Tralic-Kulenovic, L. Fiser-Jakic, D.W. Boykin, G. Karminski-Zamola, Heterocycles 55 (11) (2001) 2085–2098.
[11] N.B. Patel, A.C. Purohit, D. Rajani, Med. Chem. Res. 23 (11) (2014) 4789–4802.
[12] F. Lu, R. Hu, S. Wang, X. Guo, G. Yang, RSC Adv. 7 (2017) 4196–4202.
[13] F. Piscitellia, C. Ballatorea, A.B. Smith, Bioorg. Med. Chem. Lett 20 (2) (2010) 644–648.
[14] D.C. Dash, A. Mahapatra, R.K. Mohapatra, S. Ghosh, P. Naik, Indian J. Chem. 47A (2008) 1009–1013.
[15] R.K. ohapatra, D.C. ash, J. Kor. Chem. Soc. 54 (4) (2010) 395–401.
[16] A.I. Vogel, A Text Book of Quantitative Inorganic Analysis, Long Mans and ELBS, third ed., 1969.
[17] GaussView 5.0, Gaussian Inc., Wallingford, CT, USA), 2009.
[18] A.D. Becke, J. Chem. Phys. 98 (7) (1993) 5648–5652.
[19] C.T. Lee, W.T. Yang, R.G. Parr, Phys. Rev. B 37 (1988) 785–789.
[20] A.D. Becke, Phys. Rev. 88 (1988) 1053–1062.
[21] P.J. Hay, W.R. Wadt, J. Chem. Phys. 82 (1) (1984) 270–276.
[22] P.J. Hay, W.R. Wadt, J. Chem. Phys. 82 (1985) 284–298.
[23] P.J. Hay, W.R. Wadt, J. Chem. Phys. 82 (1985) 299–310.
[24] M.J. Frish, et al., GAUSIAN 03, Revision E.01, Gaussian Inc., Pittsburgh, PA, 2004.
[25] L.M. Podust, T.L. Poulos, M.R. Waterman, Proc. Natl. Acad. Sci. Unit. States Am. 98 (2001) 3068–3073.
[26] DS Visualizer 3.5, Accelrys Software Inc., San Diego, California, USA.
[27] The PyMOL Molecular Graphics System, Version 1.0r1, Schrödinger, LLC.
[28] D.A.E. Ella, E. Gonitzer, W. Wendelin, J. Heterocycl. Chem. 33 (2) (1996) 373–382.
[29] R.P. Singh, J.P. Tandon, Ind. J. Chem. 19A (1980) 602–609.
[30] K. Das, S.K. Gupta, V.S. Prasad, L.K. Mishra, J. Ind. Chem. Soc. 59 (1982) 334–338.
[31] K. Nakamato, Infrared Spectra of Inorganic and Coordination Compounds, John Wiley, New York, 1963.
[32] M. Mikami, I. Nakagawa, T. Shimanouchi, Spectrochim. Acta 25 (2) (1969) 365–374.
[33] T. Niyazawa, T. Shimanouchi, S. Mizushima, J. Chem. Phys. 29 (3) (1958) 611–615.
[34] J.D.S. Goulden, Spectrochim. Acta 16 (6) (1960) 715–720.
[35] A.V. Nikolaev, V.A. Lagvienko, I. Myachina, Thermal Analysis, Academic Press, New York, 1969.
[36] D. Nagakavitha, K.H. Reddy, J. Indian Chem. Soc. 92 (2015) 71–77.
[37] N. Raman, A. Kulandaisamy, K. Jayesubramanian, Indian J. Chem. 41A (2002) 942–949.
[38] C.T. Prabhakara, S.A. Patil, A.D. Kulkarni, V.H. Naik, M. Manjunatha, S.M. Kinnal, P.S. Badami, J. Photochem. Photobiol. B Biol. 148 (2015) 322–332.
[39] J.W. Visser, J. Appl. Crystallogr. 2 (1969) 89–95.
[40] P.M. de Woulff, J. Appl. Crystallogr. 1 (1968) 108–113.
[41] A. Patterson, Phys. Rev. 56 (10) (1939) 978–985.
[42] T.A. Yousef, T.H. Rakha, U. El Ayaan, G.M. Abu El Reash, J. Mol. Struct. 1007 (2012) 146–157.
[43] T.A. Yousef, G.M. Abu El-Reash, T.H. Rakha, U. El-Ayaan, Spectrochim. Acta 83 (1) (2011) 271–278.
[44] A.K. Sarangi, B.B. Mahapatra, S.K. Sethy, Chemistry Africa 1 (2018) 17–28. https://doi.org/10.1007/s42250-018-0002-z.
[45] B.B. Mahapatra, S.N. Chaulia, A.K. Sarangi, S.N. Dehury, J.R. Panda, J. Mol. Struct. (2015) 11–25. https://doi.org/10.1016/j.molstruc.2015.01.030.
[46] N.O. Can, U.A. Cevik, B.N. Saglik, S. Levent, B. Korkut, Y. Ozkay, Z.A. Kaplancikli, A.S. Koparal, J. Chem. 2017 (2017) 1–15, 9387102, https://doi.org/10.1155/2017/9387102.
[47] N.E.A. El-Gamel, J. Coord. Chem. 63 (3) (2010) 534–543.
[48] M.M.E. Shakdofa, A.N. Al-Hakimi, F.A. Elsaied, S.O.M. Alasbahi, A.M.A. Alkwlini, Bull. Chem. Soc. Ethiop. 31 (1) (2017) 75–91.